Tripathi, Tripurari S.; Lahtinen, Jouko; Karppinen, Maarit

Atomic Layer Deposition of Conducting CuS Thin Films from Elemental Sulfur

Published in:
Advanced Materials Interfaces

DOI:
10.1002/admi.201701366

Published: 01/05/2018

Document Version
Peer reviewed version

Please cite the original version:
Tripathi, T. S., Lahtinen, J., & Karppinen, M. (2018). Atomic Layer Deposition of Conducting CuS Thin Films from Elemental Sulfur. Advanced Materials Interfaces, 5(9), [1701366]. https://doi.org/10.1002/admi.201701366

WILEY-VCH

DOI: 10.1002/ ((please add manuscript number))
Article type: Full Paper

Atomic Layer Deposition of Conducting CuS Thin Films from Elemental Sulfur

Tripurari S. Tripathi,[1] *Jouko Lahtinen*[2] *and Maarit Karppinen*[1]*

*corresponding author: maarit.karppinen@aalto.fi

[1]Department of Chemistry and Materials Science, Aalto University, P.O. Box 16100, Fi-00076 Aalto, Finland

[2]Department of Applied Physics, Aalto University, P.O. Box 15100, FI-00076 Aalto, Finland

Keywords*:* Atomic layer deposition, copper(II) sulfide, sulfur, thin film

ABSTRACT: We report a facile, yet precisely controlled and efficient atomic layer deposition (ALD) process for high-quality copper(II) sulfide thin films based on elemental solid sulfur as the source for sulfur; $Cu(acac)_2$ (acac: acetylacetonate) is used as the copper precursor. In the deposition temperature range as low as 140–160 °C the process proceeds in an essentially ideal ALD manner and yields single-phase CuS thin films with appreciably high growth rate of ca. 4 Å per cycle. When the deposition temperature is increased above 160 °C the growth rate considerably increases and flake-like nanostructures evolve. All the as-deposited films are crystalline, highly conducting and specularly reflecting. Seebeck coefficient measurements confirm the p-type conducting nature of the films. The direct optical bandgap as determined from UV-visible spectroscopic measurements varies in the range of 2.40–2.54 eV, depending on the deposition temperature.

1. Introduction

Copper sulfides have attracted significant attention over the past few decades as potential material candidates for a number of advanced applications,[1,2] ranging from optoelectronics[3,4] to biomedical devices.[5-7] The early studies on copper sulfide materials were motivated by the superconductivity (T_c = 1.6 K) and the certain similarity of CuS to the copper oxide high-T_c superconductors owing to its quasi-two-dimensional layered crystal structure.[8-10] However, the more recent rapidly growing interest in copper and other metal sulfides is mostly driven by energy and photonic applications where the earth-abundant sulfide materials would be attractive low-cost alternatives to the existing materials. For example, so-called CIGS or Cu)In,Ga)$(S,Se)_2$ absorber solar cells have shown record-high cell efficiencies up to 21.7%.[11,12] Also, CuS has been considered as an interesting cathode material candidate for lithium-ion batteries.[13,14]

Copper sulfide thin films have been fabricated by various deposition techniques, such as chemical vapor deposition,[15] sputtering, spray pyrolysis,[16,17] chemical bath deposition,[18,19] and electrochemical methods.[20-22] However, in most cases the required control over the film stoichiometry and phase composition is poorly achieved due to the coexistence of several stable and metastable copper sulfide phases.[23] Moreover, fabrication of continuous copper sulfide coatings with a well-controlled morphology on high-aspect-ratio nanostructures has remained a challenge. It is here in particular where the atomic layer deposition (ALD) technique could provide us with clear advantages over the other thin-film technologies for the deposition of high-quality copper sulfide thin films for various advanced applications including the photovoltaics.[17,24,25] Atomic layer deposition is based on sequential and self-limiting gas-surface reactions, and is known to yield exceptionally homogeneous coatings in atomic-scale precision independent of the substrate geometry.

The vast majority of the metal sulfide ALD processes are based on metal-organic precursors together with hydrogen sulfide H_2S as the source of sulfur;[26] the same applies to the reported copper sulfide ALD processes as well, see Table 1. The main merit of H_2S is that it is highly reactive towards common metal precursors. However, H_2S is a flammable, corrosive and highly toxic gas, and its incorporation in the ALD technology presents several serious technical challenges. The special precautions required for the safe use of H_2S may even be one of the reasons why only 16 metal sulfide ALD processes have been so far reported during the half a century long ALD history.[26] Another drawback of the H_2S-based ALD processes is the slowness of these processes, see e.g. the growth rate values given in Table 1 for the copper sulfide processes. Moreover, majority of the reported copper sulfide processes yield Cu(I) sulfide as the main phase; hence, there is a clear interest in a new robust and efficient ALD process for high-quality Cu(II) sulfide thin films.[27]

Table 1. ALD processes for copper sulfides

Precursors	Dep. Temp. (^{0}C)	GPC (Å/cycle)	Main phase	Refs.
$[Cu(^{S}Bu\text{-}amd)]_2$ /H_2S	80–200	0.57–0.94	Cu_2S	[28-31]
$Cu(thd)_2$ /H_2S	< 170	0.4	CuS	[17,32,33]
	>170	0.2	Cu_2S	
$Cu(thd)_2$ /H_2S	125–160	0.3–0.5	Cu_xS	[24]
$Cu(acac)_2$ /H_2S	130–220	0.25	Cu_xS	[34]

Bu-amd: bis(N,N′-disec-butylacetamidinato)
thd: 2,2,6,6-tetramethyl-3,5-heptanedione
acac: acetylacetonate

Despite the fact that some of the early ALD processes employed elemental sulfur instead of H_2S as the sulfur source,[35] to the best of our knowledge no sulfur-based ALD processes have been reported for copper sulfide thin films. Here, we present a simple and efficient low-temperature ALD process for the deposition of high-quality p-type conducting CuS thin films from copper acetyl acetonate and elemental sulfur precursors, as a highly viable solution to the challenges discussed above.

2. Results and Discussion

We first explored the deposition parameters of our $Cu(acac)_2$+S process as demonstrated in **Figure 1**. In **Figure 1a** the growth-per-cycle (GPC) value, calculated from the AFM-determined film thickness value and the number of ALD cycles applied, is plotted against the precursor pulse lengths; it can be seen that the self-limiting surface saturation of the precursors is achieved with relatively short pulse lengths, as the GPC value remains constant and independent of the choice of the pulse lengths once the pulse length for $Cu(acac)_2$ is 2 s or longer. In **Figure 1**a this is demonstrated at 160 °C, but similar results were obtained for other deposition temperatures (140 and 150 °C) as well. For the rest of the depositions we fixed the pulse length to 2 s for $Cu(acac)_2$ and to 1 s for sulfur; the N_2 purge length was 4 and 2 s, respectively.

As presented in **Figure 1b**, the impact of the deposition temperature was investigated in the range from 140 to 240 °C; note that the lower limit was defined by the sublimation temperature of the $Cu(acac)_2$ precursor and the higher limit by its decomposition temperature.[36,37] It is seen that with increasing temperature the GPC value first remains constant at ca. 4 Å/cycle up to 160 °C. Interestingly, this GPC value is comparable to the lattice parameters of the CuS phase, i.e. a = b = 3.792 Å and c = 16.34 Å (JCPDS Card No. 00-06-0464), thus suggesting that the film indeed grows in a monolayer manner in this temperature range. Above 160 °C the growth rate increases monotonically until 230 °C and then decreases sharply at 240 °C, possibly due to the decomposition of copper precursor.[36,37] The reason for the increasingly high GPC values in the temperature range 160–230 °C is not known; nevertheless, the film growth process was perfectly reproducible and the resultant films were found to be highly homogeneous. Finally we confirmed that the film thickness increases in a linear manner against the number of deposition cycles, as expected for an ideal ALD process; in **Figure 1c** we show this at the deposition temperature 160 °C, but similar results were obtained at other temperatures (140 and 150 °C) as well.

All our as-deposited films were crystalline independent of the deposition temperature; GIXRD patterns are displayed in **Figure 2**. The sharp diffraction peaks manifest the high degree of crystallinity of the films. All the reflection peaks were readily indexed with the hexagonal CuS structure (JCPDS card 00-006-0464) except for the film deposited at 240 ºC for which minor amounts of the Cu_2S phase (JCPDS card 03-065-2980) appeared. No other impurity peaks or peaks due to some intermediate $Cu_{1+x}S$ phases were seen for any of the samples. An interesting observation from **Figure 2** is that the relative intensity of the 006 CuS peak increases with increasing deposition temperature indicating towards gradual increase/change in the preferred orientation.

We also calculated the grain size of the nanocrystals in our polycrystalline CuS thin films from the GIXRD data using the Scherrer equation and the FWHM of the 110 CuS peak. It was seen that the crystallite size remains essentially constant around 45 nm for the deposition temperature range 140–160 ^{o}C (where also the GPC value remains constant), but then above 160 ^{o}C decreases until 200 ^{o}C to then again increase onward.

In **Figure 3** we show the XRR patterns (together with the derivatives of the patterns in the inset) recorded for our CuS films deposited at different temperatures. As is evident from the main figure, the films do not show the fringe pattern commonly observed for thin films with smooth surfaces. The lack of the fringes is due to the surface roughness of the films which is rather typical for highly crystalline ALD films;[38] the surface roughness is also seen from the AFM images in **Figure 4**. It is well known that XRR patterns are very sensitive to the surface roughness, such that the fringes are unlikely to be distinguished when the roughness exceeds 2–3 nm.[39] Therefore we could not use the XRR data to confirm the AFM-determined film thickness values; however, the patterns contain information on the electronic density profile perpendicular to the film surface, and reveal hence useful information of the film density.[40]

We calculated the film densities from the so-called critical angles (below which the incident X-rays are totally reflected from the surface); these were best determined from the derivative XRR curves shown in the right inset of **Figure 3**. In general, the higher the electron density is, the higher is the critical angle.[40,41] For our ALD CuS thin films the critical angle shifts to the lower angles as the deposition temperature increases indicating that the films deposited at the higher temperatures are less dense than those deposited at the lower temperatures. As displayed in the left inset of **Figure 3**, the estimated density is 3.8 g/cm^3 for the films deposited in the range 140–160 ^{o}C; this is comparable to the bulk density of 4.6 g/cm^3 reported for hexagonal CuS structure (JCPDS card 00-006-0464). For the films deposited at the higher temperatures the density value monotonically decreases down to 2.4 g/cm^3.

We used SEM and AFM to further investigate the surface morphologies of the films, see **Figure 4**. It is clearly seen that the films deposited at lower temperatures are smoother than those deposited at higher temperatures. As the deposition temperature increases, the RMS roughness value increases from 5 nm for the film deposited at 140 ^{o}C to even ca. 50 nm for the films deposited at the highest temperatures. These very high surface roughness values could explain the low density values determined for the films deposited at the highest temperatures. The SEM images further show that several different morphological structures evolve with increasing deposition temperature: dense rice-like nanograins for films deposited at 140–160 ^{o}C, nanorods at 180–200 ^{o}C and nanoflakes at 220–230 ^{o}C. At 240 ^{o}C the flakes are partly dissolved; this is accompanied with the appearance of larger amounts of the Cu_2S secondary phase (according to GIXRD) and probably also the partial decomposition of the copper precursor.

To probe the chemical composition of the films and the oxidation states of the constituent elements, XPS spectra were collected for representative samples; in **Figure 5** high-resolution spectra of the Cu 2p and S 2p regions are shown for a thin film deposited at 150 ^{o}C. The Cu

$2p_{3/2}$ and Cu $2p_{1/2}$ peaks located at 932.2 and 952.1 eV, respectively, are indicative of the divalent state of copper and agree well with the data previously reported for CuS in literature.[42-44] The S 2p region (inset of **Figure 5**) presents the S $2p_{3/2}$ and S $2p_{1/2}$ spin–orbit doublet at binding energies 161.5 and 162.5 eV, respectively, and thus separated by 1.0 eV, in agreement with literature data for CuS.[42,45] Also, the atomic ratio for Cu and S as estimated from the relative intensities of the Cu 2p and S 2p peaks corresponds to the CuS phase. However, a distinct C 2p peak was seen as well (not shown here) for all the samples investigated indicating that there is some carbon impurity in our CuS films possibly of the order of few atomic percentages (seemingly independent of the deposition temperature). We believe it could be reduced by choosing in future works a longer purge time than the one chosen for present depositions for the copper precursor.

To estimate the optical bandgaps, UV-Vis absorbance measurements were carried out for our CuS thin films deposited at different temperatures (on borosilicate glass substrate). The absorption coefficient (α) data calculated from the UV-Vis spectra using the formula $\alpha = 2.303\ A / t$, where A is absorbance and t the film thickness, are displayed in the inset (a) of **Figure 6**. The onset of the sharp rise seen in the absorption coefficient for each sample around 550 nm corresponds to the room-temperature optical bandgap energy of the film. The equation $(\alpha h\nu)^{1/n} = K(h\nu - E_g)$, where ν is the frequency of incident radiation and K is an arbitrary constant, was then used to determine the exact optical bandgap value. We initially fitted the data for both the direct and indirect bandgaps; a value of ½ and 2 was given to n, respectively. A clearly better fit was achieved with n = ½ indicating towards a direct bandgap in our CuS films in accordance with the latest literature data for CuS.[2,46-49] As seen from the Tauc plots in the main **Figure 6** and the inset (b), the direct bandgap of the films varies in the range of 2.40–2.54 eV, depending on the deposition temperature, first slightly increasing and then decreasing with increasing deposition temperature. We believe this may be related to the changes in the size and

morphology of crystallites. In overall, the obtained optical bandgap values are consistent with the values reported in previous studies for bulk and thin film samples of CuS.[50,51]

Finally, in **Figure 7** we show the electrical transport properties, i.e. resistivity and Seebeck coefficient, of the films as a function of temperature. It is widely believed that while Cu_2S is a p-type semiconductor, pure/stoichiometric CuS should exhibit a metallic-type conduction behavior; in nonstoichiometric $Cu_{1+x}S$ the p-type conduction is attributed to the free holes from copper acceptor vacancies that increase as x decreases from 1 to 0. However, there are several reports on semiconducting CuS thin films as well.[52,53] Our CuS films show a perfect metallic conduction behavior ($d\rho/dT > 0$) for the whole temperature range measured, i.e. 77–400 K. The absolute resistivity values of the films increase substantially with increasing deposition temperature. Carbon contamination might affect the resistivity values; since we did not observe any significant differences in carbon content for our CuS films deposited at different temperatures we tentatively assume that the large changes in film density (from 3.8 to 2.4 g/cm^3 with increasing deposition temperature) could be the dominant reason for the observed changes in resistivity. The minimum room-temperature resistivity of 0.63 μW-m is seen for the CuS film deposited at 140 ^oC. In Seebeck coefficient data the broad minimum around 250–350 K is quite similar to the minimum observed in metals such as copper, silver, etc., after phonon drag peak at low temperatures. Here, however it is comparatively broad, and may be rather related to the morphological changes observed in the SEM images and grain boundary scatterings that may play an important role in electrical transport processes. Moreover, the positive Seebeck coefficient values confirm the p-type conducting nature of the films as expected based on previous reports for CuS.

3. Conclusions

We have demonstrated a novel ALD process for copper sulfide thin films utilizing elemental S instead of the commonly employed H_2S as the source of sulfur. Combined with $Cu(acac)_2$ as the source of copper, the new process yields single-phase highly crystalline CuS thin films through self-limiting surface reactions at as low deposition temperatures as 140–160 °C. A small carbon impurity is revealed from XPS measurements; nevertheless, resistivity and Seebeck coefficient measurements confirm p-type metallic-like conductivity for the films, as expected for high-quality CuS films. We believe that by using essentially longer N_2 purge periods after the $Cu(acac)_2$ precursor pulse it could be possible to reduce the carbon content; this should be systematically investigated in future works.

A highly attractive feature of our $Cu(acac)_2$+S process is the high growth rate of the films; in the deposition temperature range of 140–160 °C the GPC value was ca. 4 Å/cycle which is an order of magnitude higher than the values typically reported for various H_2S based copper sulfide ALD processes. From the basic sulfur chemistry we know that depending on the conditions the sulfur vapor may contain not only atomic S, but also larger units, such as S_2, S_4, S_6 or S_8.[54] Hence, it is possible that during the sulfur precursor pulse the film surface may be exposed to an excessive number of sulfur atoms per the reactive site; tentatively, we believe that this could explain the appreciably high GPC values.

The films deposited at 140–160 °C exhibited appreciably smooth homogeneous surfaces which are not always the case for in-situ crystalline ALD films. When the deposition temperature was increased above 160 °C the morphology changed from rice-like nanograins first to nanorods and then at the highest deposition temperatures to nanoflakes. Simultaneously the surface became remarkably rough, and very high GPC values were measured. Nevertheless, the films were of the single CuS phase up to the deposition temperature of 230 °C above which a trace of the Cu_2S phase appeared. From optical measurements, the direct optical bandgap

varied in the range 2.40–2.54 eV, slightly depending on deposition temperature from 140 to 240 ^{o}C. All the films exhibited metallic-like electrical conductivity.

Finally we like to emphasize that metal sulfide ALD processes based on elemental sulfur have been little explored. For comparison, it is interesting to note that there are several reports on the preparation of metal sulfide nanoparticles from metalorganic precursors and elemental sulfur using solution process techniques.[55,56] In particular, preparation of CuS nanoparticles have been reported using $Cu(acac)_2$ and elemental sulfur in oleyamine solution.]51,57[We positively believe that our promising results with the $Cu(acac)_2$+S process could motivate researchers to develop sulfur-based ALD processes for other metals as well, and even similar processes based on elemental selenium or tellurium for metal chalcogenides as these materials are gaining increasing interest in many advanced technologies.

4. Experimental Section

The CuS thin-film depositions were carried out in a commercial flow-type F-120 reactor manufactured by ASM Microchemistry Ltd (Espoo, Finland).[58] The precursor vapors were consecutively pulsed into the reactor while high purity (99.999%(nitrogen was used as a carrier and purging gas. The precursor powders were procured from commercial sources, i.e. $Cu(acac)_2$ from STREM chemicals (purity 97%) and elemental sulfur from Sigma Aldrich (purity 99.999%) and pulsed into the reactor in a sequence. The sublimation temperatures were: 140 ^{o}C for $Cu(acac)_2$ and 115 ^{o}C for S, and the pulse time was varied between 1–5 s. In each case, the successive N_2 gas pulse length for purging was 2 s longer than the precursor pulse. The total reactor pressure varied between 3–4 mbar during the depositions. The films were deposited on 3.5×3.5 cm^2 borosilicate glass and silicon substrates (without removing the native oxide layer in the latter case). It should be noted that $Cu(acac)_2$ was selected as the source for copper as it

is a common copper precursor used in ALD processes of many Cu compunds; in our preliminary experiments $Cu(thd)_2$ was tested as well but it did not react with elemental sulfur.

Crystallinity and phase composition of the films were investigated with grazing incidence X-ray diffraction (GIXRD; PANanalytical model X'pert Pro diffractometer; CuK_α radiation). The same diffractometer was used for the X-ray reflectivity)XRR(measurements. The films were highly crystalline and therefore the surface roughness was too high for the XRR data to be used for film thickness determination; however, the XRR data were used to estimate the film densities from the critical angles. The film thicknesses were estimated with atomic force microscopy (AFM; TopoMetrix Explorer) using the cantilever tip jump technique;[59] the as-deposited films were stable even when left in ambient conditions for several days. The surface topography and root-mean-square (RMS) roughness measurements were performed using the same AFM in the contact mode. Surface morphology of the films was additionally examined by scanning electron microscopy (SEM; Zeiss-Sigma VP, resolution 1.3 nm @ 20 kV).

The chemical composition of the films and in particular the chemical state of copper were investigated for representative films by X-ray photoelectron spectroscopy (XPS; Kratos Axis Ultra ESCA system with a dual anode Mg and Al K_α source and a monochromatic Al K_α source). Before the XPS analysis the film surface was sputtered with Ar^+ for 30 s to remove any surface contaminants, as the films had been stored in ambient conditions for several weeks.

For the physical-property characterization, both UV-vis absorbance (Perkin Elmer UV/VIS Spectrometer, Model: Lambda 2) and electrical transport measurements were performed. For the electrical transport measurements the films were deposited on borosilicate glass substrates. Temperature-dependent dc electrical resistivity measurements were performed on square substrates of 1x1 cm^2 in linear four-probe geometry. The spacing between the probes was fixed to 1 mm and the electrical contacts were made using colloidal silver paste (Ted Pella. Inc. USA). The films were put upside down on the contacts and spring pressed to avoid any

loose connection during the temperature-sweep measurements. Seebeck measurements were conducted using a homemade setup based on equilibrium principle.[60]

Acknowledgements

The present work has received funding from the Academy of Finland through the Strategic Research Council (grant number 303452) and the Mineral Resources and Material Substitution Programme (grant number 292431).

Received: ((will be filled in by the editorial staff))
Revised: ((will be filled in by the editorial staff))
Published online: ((will be filled in by the editorial staff))

]1[S. Sun, P. Li, S. Liang, Z. Yang, *Nanoscale* **2017**, *9*, 11357.
]2[P. Roy, S. K. Srivastava, *CrystEngComm.* **2015**, *17*, 7801.
]3[X. L. Yu, C. B.Cao, H. S. Zhu, Q. S. Li, C. L. Liu, Q. H. Gong, *Adv. Funct. Mater.* **2007**, *17*, 1397.
]4[Y. B. Lou, A. C. S. Samia, J. Cowen, K. Banger, X. B. Chen, H. Lee, C. Burda, *Phys. Chem. Chem. Phys*. **2003**, *5*, 1091.
]5[Q. W. Tian, M. H. Tang, Y. G. Sun, R. J. Zou, Z. G. Chen, M. F. Zhu, S. P. Yang, J. L.Wang, J. H. Wang, J. Q. Hu, *Adv. Mater.* **2011**, *23*, 3542.
]6[S. Goel, F. Chen, W. Cai, *Small* **2014**, *10*, 631.
]7[K. Ding, J. Zeng, L. Jing, R. Qiao, C. Liu, M. Jiao, Z. Lib, M. Gao, *Nanoscale* **2015**, *7*, 11075.
]8[W. Meissner, *Z. Phys*. **1929**, *58*, 570.
]9[W. Buckel, R. Hilsh, *Z. Phys*. **1950**, *128*, 324.
]10[A. J. Aguiar, C. L. S. Lima, Y. P. Yadava, L. D. A. Tellez, J. M. Ferreira, E. Montarroyos, *Physica C*, **2000**, *341*, 593.
]11[P. Jackson, D. Hariskos, R. Wuerz, O. Kiowski, A. Bauer, T. M. Friedlmeier, M. Powalla, *Phys. Status Solidi RRL* **2015**, *8*, 28.
]12[A. Chirilă, P. Reinhard, F. Pianezzi, P. Bloesch, A. R. Uhl, C. Fella, L. Kranz, D. Keller, C. Gretener, H. Hagendorfer, D. Jaeger, R. Erni, S. Nishiwaki, S. Buecheler, A. N. Tiwari, *Nature Mater*. **2013**, *12*, 1107.
]13[M. Nagarathinam, K. Saravanan, W. L. Leong, P. Balaya, J. J. Vittal, *Cryst. Growth Des*. **2009**, *9*, 4461.
]14[H. Mazor, D. Golodnitsky, L. Burstein, E. Peleda, *Electrochem. Solid-State Lett*. **2009**, *12*, A232.
]15[M. Kemmler, M. Lazell, P. O'Brien, D. J. Otway, J. H. Park, J. R. Walsh, *J. Mater. Sci.: Materials in Electronics* **2002**, *13*, 531.
]16[J. Vedel, P. Cowache, M. Dechraoni, *Rev. Phys. Appl*. **1980**, *15*, 1521.
]17[L. Reijnen, B. Meester, F. DeLang, J. Schoonmam, A. Goossens, *Chem. Mater*. **2005**, *17*, 2724.
]18[N. Mukherjee, A. Sinha, G. G. Khan, D. Chandra, A. Bhaumik, A. Mondal, *Mater. Res. Bull*. **2011**, *46*, 6.
]19[M. Xina, K. W. Lia, H. Wang, *Appl. Surf. Sci*. **2009**, *256*, 1436.
]20[S. Caporali, A. Tolstogouzov, O. M. N. D. Teodoro, M. Innocenti, F. D. Benedetto, S. Cinotti, R. A. Picca, M. C. Sportelli, N. Cioff, *Sol. Energy Mater. Sol. Cells* **2015**, *138*, 9.
]21[A. Giaccherini, I. Bencistà, S. Cinotti, G. Montegrossi, A. Guerri, F. D. Benedetto, A. Lavacchi, M. L. Foresti, R. Felici, F. Carlà, M. Innocenti, *ECS Trans.* **2014**, *58*, 35.
]22[R. D. Engelken, H. E. McCloud, *J. Electrochem. Soc.* **1985**, *132*, 567.
]23[R. J. Goble, *Can. Mineral*. **1985**, *23*, 61.
]24[J. Johansson, J. Kostamo, M. Karppinen, L. Niinistö, *J. Mater.Chem*. **2002**, *12*, 1022.
]25[C. Guerra-Nunez, H. G. Park, I. Utke, Chapter 4: Atomic Layer Deposition for Surface and Interface Engineering in Nanostructured Photovoltaic Devices. In: *Atomic Layer Deposition in Energy Conversion Applications*, Bachmann, J.)Ed.(; **2017**, Wiley-VCH Vellag & Co, Weinheim, Germany.
]26[N. P. Dasgupta, X. Meng, J. W. Elam, A. B. F. Martinson, *Acc. Chem. Res*. **2015**, *48*, 341.
]27[T. S. Tripathi, M. Karppinen, *Adv. Mater. Interfaces* **2017**, 1700300.
]28[A. B. F. Martinson, J. W. Elam, M. J. Pellin, *Appl. Phys. Lett.* **2009**, *94*, 123107.
]29[S. C. Riha, S. Jin, S. V. Baryshev, E. Thimsen, G. P. Wiederrecht, A. B. F. Martinson, *ACS Appl. Mater. Interfaces* **2013**, *5*, 10302.
]30[A. B. F. Martinson, S. C. Riha, E. Thimsen, J. W. Elam, M. J. Pellin, *Energy Environ. Sci*. **2013**, *6*, 1868.
]31[E. Thimsen, Q. Peng, A. B. F. Martinson, M. J. Pellin, J. W. Elam, *Chem. Mater*. **2011**, *23*, 4411.
]32[L. Reijnen, B. Meester, A. Goossens, J. Schoonman, *Mater. Sci. Eng. C* **2002**, *19*, 311.
]33[L. Reijnen, B. Meester, A. Goossens, J. Schoonman, *Chem. Vap. Deposition* **2003**, *9*, 15.
]34[N. Schneider, D. Lincot, F. Donsanti, *Thin Solid Films* **2016**, *600*, 103.
]35[T. Suntola, J. Hyvärinen, *Annu. Rev. Mater. Sci*. **1985**, *15*, 177.
]36[A. F. Bykov, P. P. Semyannikov, I. K. Igumenov, *J. Therm. Anal.* **1992**, *38*, 1463.

]37[A. E. Turgambaeva, A. F. Bykov, I. K. Igumenov, *Thermochimica Acta* **1995**, *256*, 443.
]38[Z. Giedraityte, O. Lopez-Acevedo, L. A. E. Leal, V. Pale, J. Sainio, T. S. Tripathi, M. Karppinen, *J. Phys. Chem. C* **2016**, *120*, 26342.
]39[P. LaPuma, M. Zimmermann, Good Diffraction Practice Webinar Series, X-ray Reflectometry *www.bruker-webinars.com* Jul 21, **2010**.
]40[L. G. Parratt, *Phys. Rev*. **1954**, *95*, 359.
]41[K. Stoev, K. Sakurai, *The Rigaku Journal* **1997**, *14(2)*, 22.
]42[Ch. D. Wagner, A. V. Naumkin, A. K. Vass, J. W. Allison, C. J. Powell, J. R. Rumble Jr., *NIST Standard Reference* Database 20, Version 3.4.
]43[J. Xuchuan, X. Yi, L. Jun, H. Wei, Z. Liying, Q. Yitai, *J. Mater. Chem*. **2000**, *10*, 2193.
]44[Ch. D. Wagner, W. W. Riggs, L. E. Davis, J. F. Moulder, G. E. Muilenberg, G. E. *Handbook of X-Ray Photoelectron Spectroscopy*, Perkin-Elmer Corporation, Physical Electronics Division, USA, **1979**.
]45[V. Krylova, A. Andrulevicius, *Int. J. Photoenergy* **2009**, *2009*, 304308.
[46] M. A. Yildirim, A.- Ates, A. Astam, *Physica E* **2009**, *41* 1365.
[47] F. I. Ezema, M.N. Nnabuchi, R. U. Osuji, *Trends Appl. Sci. Res.* **2006**, *1*, 467.
[48] W. Xu, S. Zhu, Y. Liang, Z. Li, Z. Cui, X. Yang, A. Inoue, *Sci. Rep.* **2015**, *5*, 18125.
[49] J. Kundu, D. Pradhan, *New J. Chem*. **2013**, *37*, 1470.
]50[P. Zhang, L. Gao, *J. Mater. Chem*. **2003**, *13*, 2007.
]51[H. T. Zhang, G. Wu, X. H. Chen, *Mater. Chem. Phys.* **2006**, *98*, 298.
]52[S. D. Sartale, C. D. Lokhande, *Mater. Chem. Phys.* **2000**, *65*, 63.
]53[S. H. Chaki, M. P. Deshpande, J. P. Tailor, *Thin Solid Films* **2014**, *550*, 291.
]54[R. H. Petrucci, R. H. *General Chemistry, Principles & Modern Applications.* Macmillan Publishing Company, Ninth Edition. Page 930–937. Karchmer, J. H. The Analytical Chemistry of Sulfur and its Compounds. New York: John Wiley & Sons, Inc., **1970**.
]55[M. J. Turo, J. E. Macdonald, *ACS Nano* **2014**, *8*, 10205.
]56[A. L. Abdelhady, K. Ramasamy, M. A. Malik, P. O'Brien, S. J. Haigh, J. Rafterya, *J. Mater. Chem*. **2011**, *21*, 17888.
]57[Y. Kim, K. Y. Park, D. M. Jang, Y. M. Song, H. S. Kim, Y. J. Cho, Y. Myung, J. Park, *J. Phys. Chem. C* **2010**, *114*, 22141.
]58[L. Niinistö, Curr. Opin. Solid State Mater. Sci. **1998**, *3*, 147.
]59[T. S. Tripathi, M. Karppinen, *Chem. Mater*. **2017**, *29*, 1230.
]60[T. S. Tripathi, M. Bala, K. Asokan, *Rev. Sci. Instrum*. **2014**, *85*, 085115.

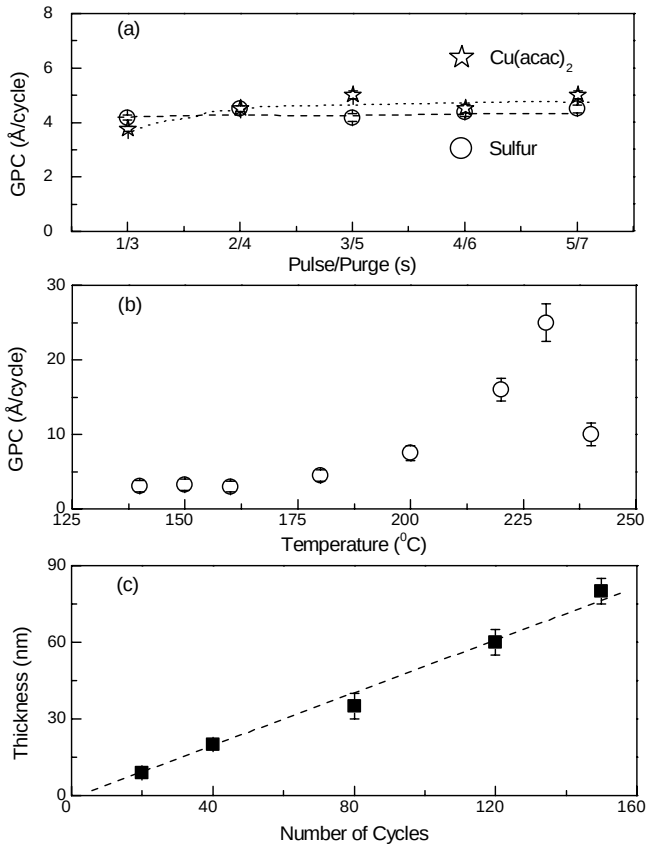

Figure 1. Optimization of the deposition parameters: (a) GPC versus precursor pulse lengths, (b) GPC versus deposition temperature, and (c) film thickness versus number of ALD cycles. In (a) and (c), the deposition temperature was 160 °C. Note that in (a) the purge time was increased together with increasing precursor pulse time such that the purge time was always longer than the precurcor pulse time to ensure the complete removal oft he precursor excess and the reaction by-products.

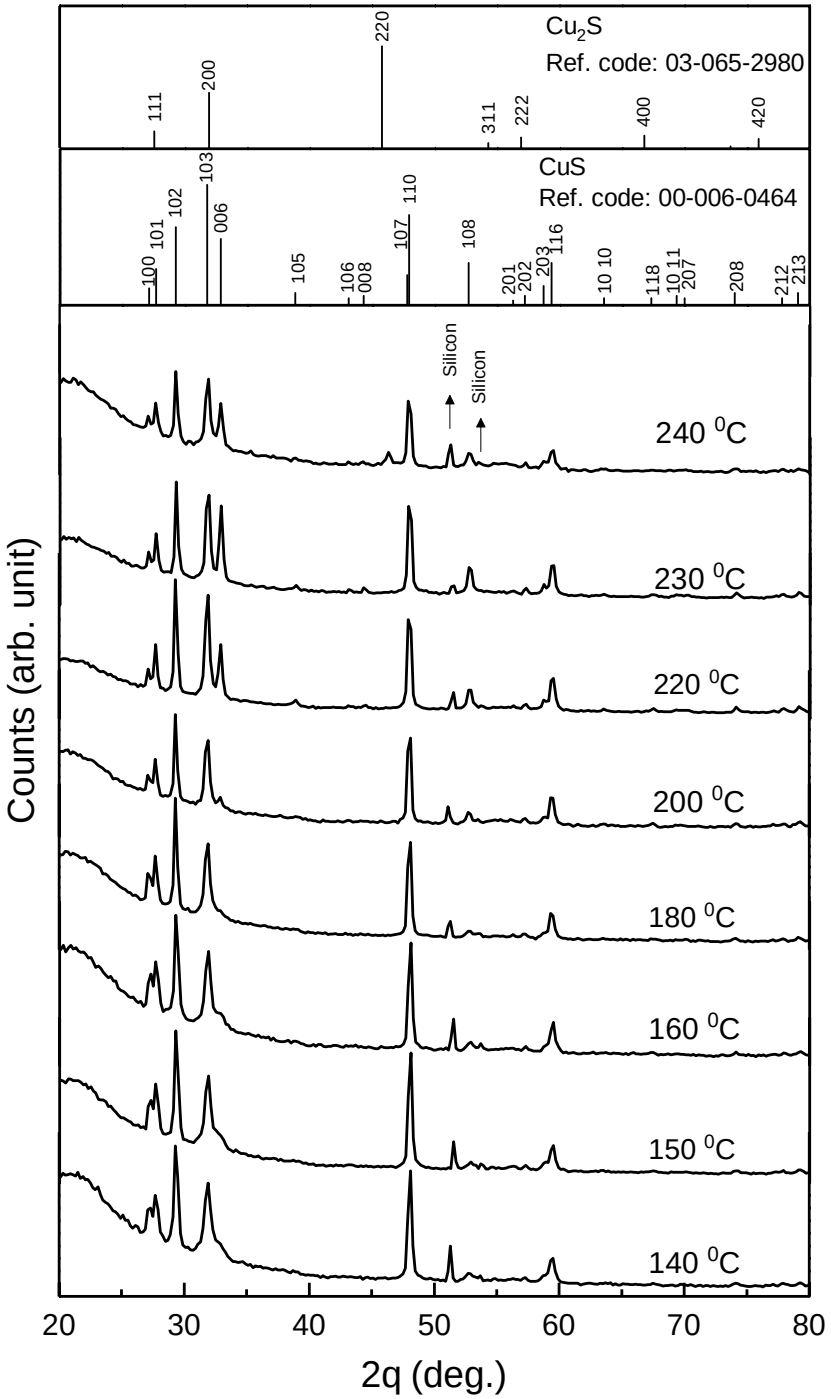

Figure 2. XRD patterns for the copper sulfide thin films deposited at different temperatures.

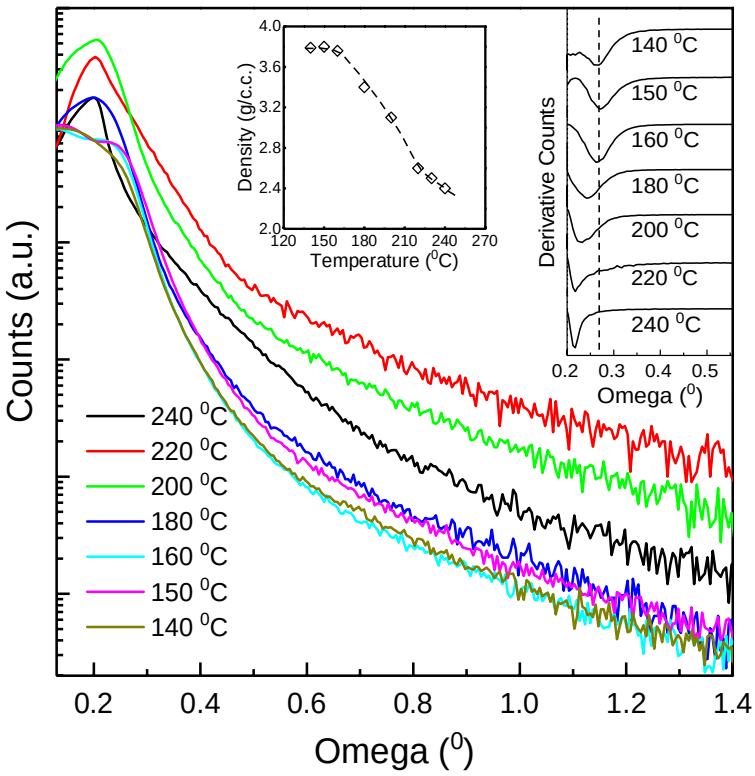

Figure 3. XRR patterns for the copper sulfide thin films deposited at different temperatures; derivative plots in the inset.

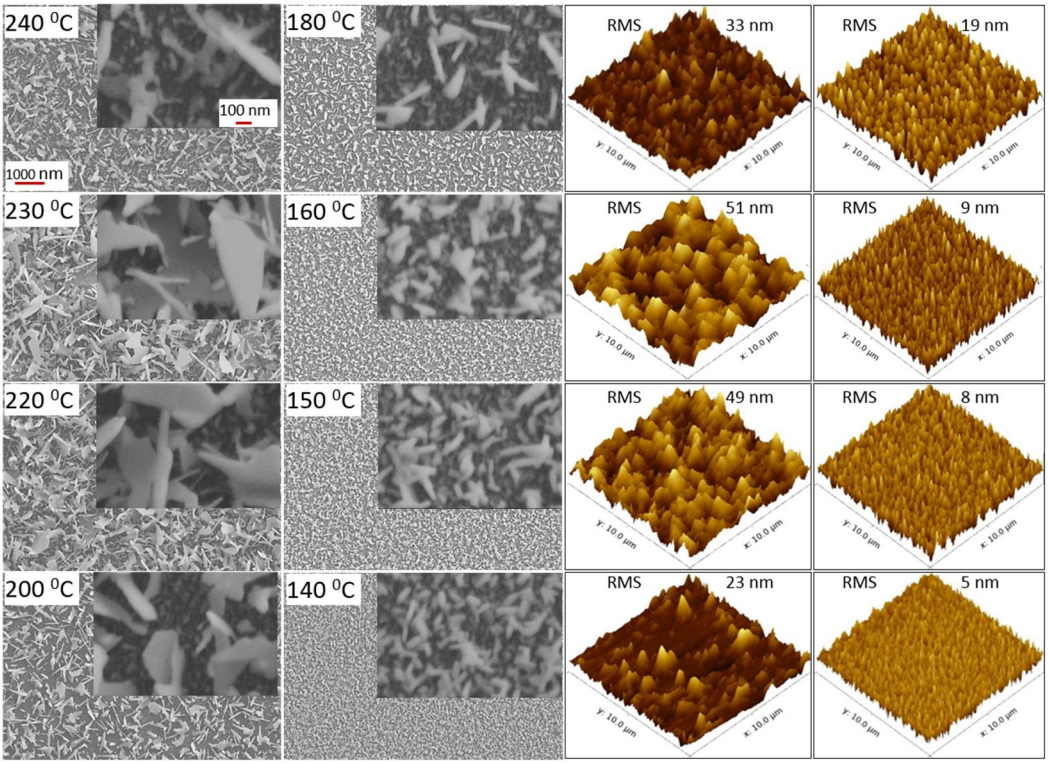

Figure 4. SEM (left) and AFM (right) images for the copper sulfide thin films deposited at different temperatures.

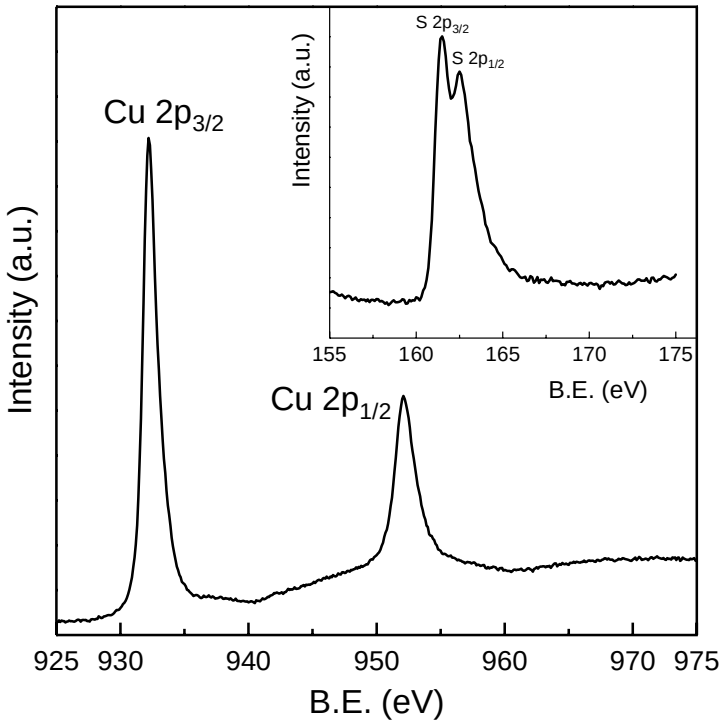

Figure 5. High-resolution XPS spectra for a copper sulfide thin film deposited at 150 ^{o}C, recorded after sputtering the film surface with Ar for 30 s.

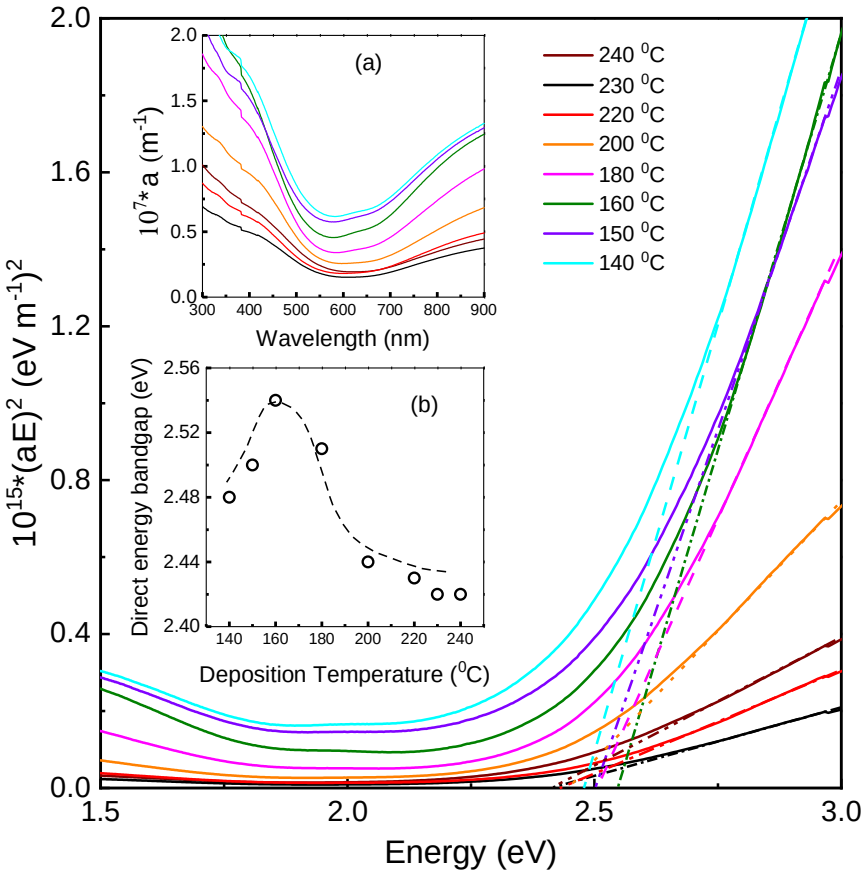

Figure 6. Tauc plots for the determination of the direct bandgap for the copper sulfide thin films deposited at different temperatures. In each case the extrapolated interception of the linear portion of the curve with the energy axis gives the optical bandgap of the film. Inset (a) displays the absorption coefficient of the films as a function of wavelength. Inset (b) shows the dependence of the bandgap on the deposition temperature; the dotted curves are for a guide to the eyes.

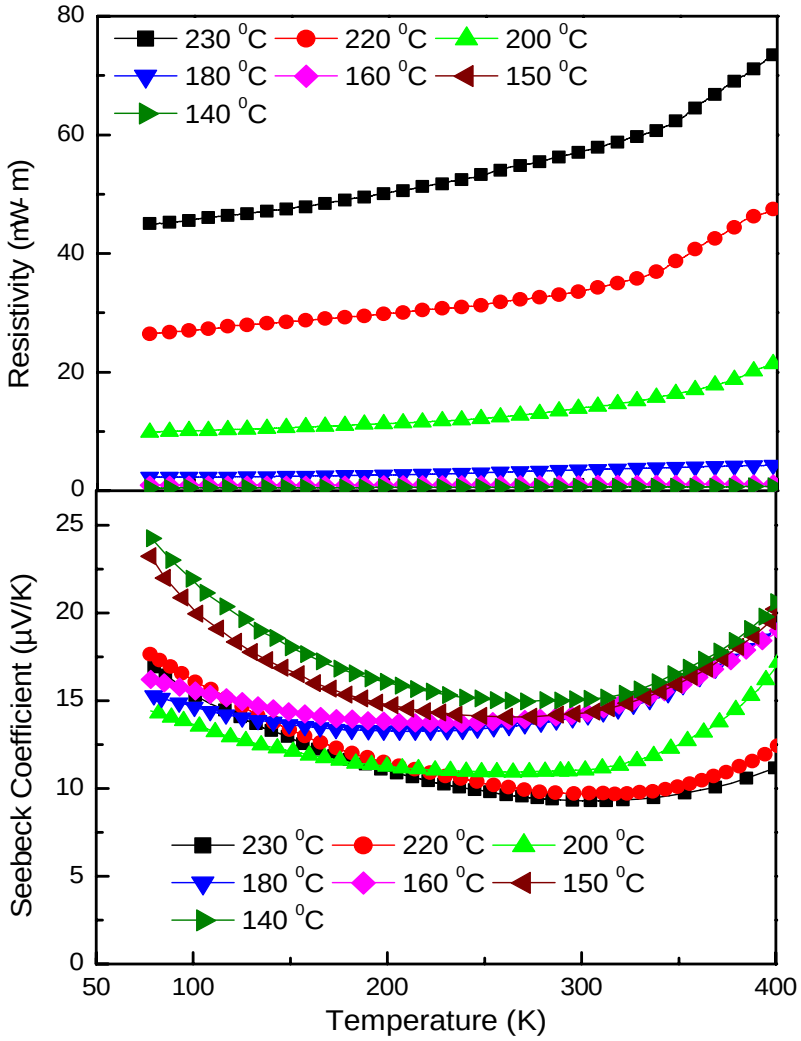

Figure 7. Electrical resistivity and Seebeck coefficient of the copper sulfide thin films deposited at different temperatures.

TOC

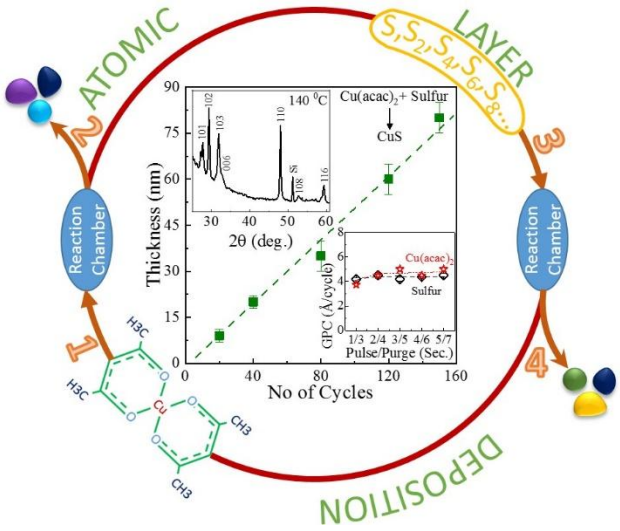
ATOMIC
LAYER
DEPOSITION
Reaction Chamber
Reaction Chamber
1
2
3
4
Thickness (nm)
No of Cycles
140 °C
Cu(acac)2+ Sulfur
CuS
2θ (deg.)
GPC (Å/cycle)
Pulse/Purge (Sec.)
Cu(acac)2
Sulfur